Supporting Information for "The intersection of field-limited density of states and matter: Nanophotonic control of fluorescence energy transfer"

Haley W. Jones,[a,b] Yuriy Bandera,[a,b] and Stephen H. Foulger[a,b,c*]

Supporting Text, Figures, and Tables

Photophysical properties of the individual emitters

Optical absorbance spectra of the anthracene, naphthalimide, and rhodamine B derivatives (AMMA, NMMA, and RMMA, respectively) in toluene are presented in **Figure S1**. A small peak at 334 nm and three large peaks at 350 nm, 368 nm, and 388 nm were detected in the absorbance spectra of AMMA in toluene. One broad peak centered at 401 nm was detected in the absorbance spectra of NMMA in toluene. A peak with a maximum at 565 nm and a shoulder at ca. 523 nm was detected in the absorbance spectra of RMMA in toluene.

Photoluminescence excitation (PLE) and photoluminescence (PL) spectra of AMMA, NMMA, and RMMA in toluene are presented in **Figure S2**. The PLE spectra of AMMA when monitored at 415 nm exhibited a small peak at ca. 335 nm and three larger peaks at 350 nm, 367 nm, and 387 nm. When excited at 367 nm, three large peaks were detected in the PL emission of AMMA at 392 nm, 414 nm, and 439 nm accompanied by a small peak at ca. 467 nm. The PLE spectra of NMMA when monitored at 496 nm exhibited a maximum peak at 396 nm. When excited at 396 nm, a maximum PL emission at 496 nm was detected. The PLE spectra of RMMA when monitored at 600 nm exhibited a small shoulder at ca. 523 nm and a maximum peak at 554 nm. When excited at 530 nm, a maximum PL emission at 578 nm was detected.

The quantum yield (QY) of AMMA and NMMA in toluene were estimated using the comparative method[1]. Quinine sulfate in 0.5 M H_2SO_4 (ϕ = 0.53) was chosen as a standard for AMMA due to the large spectral overlap with the absorption and emission characteristics of the AMMA emitter in toluene[2]. This allowed for the use of a constant excitation wavelength (367 nm) for all measurements. Absorbance spectra of quinine sulfate in 0.5 M H_2SO_4 and AMMA in toluene are presented in **Figure S3**a-b, respectively. A series of dilutions of quinine sulfate in 0.5 M H_2SO_4 and AMMA in toluene was performed such that, in each case, the absorbance at 367 nm ranged from 0.1 - 0.02. The integrated fluorescence intensity of quinine sulfate and AMMA corresponding to the series of dilutions in each respective solvent is presented in **Figure S3**c, where a linear trendline was fit to each series. A comparison of the gradient of the trendline fit to quinine sulfate and AMMA ($Grad_Q$ and $Grad_A$, respectively) was utilized to estimate the QY of AMMA in toluene (ϕ_A) by **Equation S1**.

$$\phi_A = \phi_Q \times \frac{Grad_A}{Grad_Q} \times (\frac{n_A}{n_Q})^2 \quad \text{(S1)}$$

The refractive index of the respective solvents used for quinine sulfate (n_Q) and AMMA (n_A) were accounted for in the estimation, where n_Q (0.5 M H_2SO_4) = 1.346 and n_A (toluene) = 1.4968. Through this comparison, ϕ_A in toluene was estimated to be 0.36 $\pm$ 5%. Using a similar procedure described in a previous report[3], the QY of NMMA in toluene was estimated to be 0.54 $\pm$ 5%, where coumarin 30 in acetonitrile (ϕ = 0.67)[4] was utilized as a standard for NMMA in toluene (cf. **Figure S3d-f**).

Using the quantum yield and emission spectra of the donors (AMMA and NMMA) in toluene and the absorbance spectra of the acceptors (NMMA and RMMA) in toluene, the Förster distance (R_0) between each Förster resonance energy transfer (FRET) pair could be estimated. R_0 refers to the distance between donor/acceptor molecules at which the energy transfer efficiency is 50%. The R_0 of the AMMA/NMMA FRET pair was estimated to be 2.58 nm and the R_0 of the NMMA/RMMA FRET pair was estimated to be 3.11 nm. Additionally, the R_0 of AMMA and RMMA was estimated to be 1.41 nm. While there is potential for FRET between AMMA/RMMA, energy transfer from AMMA to RMMA is less probable than AMMA to NMMA due to the shorter R_0 of AMMA/RMMA compared to that of AMMA/NMMA.

A time-correlated single photon counting (TCSPC) technique was utilized to monitor the fluorescence lifetime of each emitter at the wavelength of their maximum emission when excited with a 370 nm pulsed NanoLED source. It should be noted that a significantly larger concentration of RMMA (19.4 mM) in toluene than that of AMMA (6.0 μM) and NMMA (8.5 μM) was required to obtain sufficient signal when excited with a 370 nm source, causing a red-shift in the maximum emission. Fluorescence decay profiles (n=3) of AMMA, NMMA, and RMMA in toluene are shown in **Figure S4** (cf. **Table S1**). Decay profiles of AMMA and NMMA were both exponential and fit well to a single decay component (τ_1). The decay profile of RMMA was nonexponential was fit well assuming two decay components (τ_{1-2}). The fluorescence lifetime of AMMA in toluene at 415 nm was 4.6 ns $\pm$ 0.02 ns. The fluorescence lifetime of NMMA in toluene at 496 nm was 7.9 ns $\pm$ 0.01 ns. The two fluorescence lifetime components of RMMA in toluene at 601 nm were 1.21 ns $\pm$ 0.04 ns and 3.28 ns $\pm$ 0.06 ns.

Confirmation of FRET between emitters

To confirm Förster resonance energy transfer (FRET) occurs between the AMMA/NMMA emitters and NMMA/RMMA emitters, PL

* foulger@clemson.edu
[a] Center for Optical Materials Science and Engineering Technologies (COMSET), Clemson University, Anderson, SC, 29625
[b] Department of Materials Science and Engineering, Clemson University, Clemson, SC 29634
[c] Department of Bioengineering, Clemson University, Clemson, SC 29634

spectra of each donor or acceptor emitter was obtained before and after mixing with their respective FRET pair. Changes in emission intensity of each emitter were estimated by integrating the PL spectra attributed to each emitter. The PL spectra of AMMA and NMMA in acetone before and after mixing is presented in **Figure S5a**. After mixing, the emission of the AMMA donor was decreased by -23% while the emission of the NMMA acceptor was enhanced by +6%, indicating that FRET does occur between the AMMA/NMMA pair. The PL spectra of NMMA and RMMA in acetone before and after mixing is presented in **Figure S5b**. After mixing, the emission of the NMMA donor was decreased by -15% while the emission of the RMMA acceptor was significantly enhanced by +167%, indicating that FRET does occur between the NMMA/RMMA pair.

Incorporation and quantification of the emitters in the n_1 nanoparticles

Optical absorbance of AMMA, NMMA, and RMMA in aniline at concentrations of 5 μg/mL, 2.5 μg/mL, and 1 μg/mL are shown in **Figure S6a-c**. The absorbance spectra of AMMA in aniline has three distinct peaks at 352 nm, 371 nm, and 391 nm, NMMA in aniline has a broad peak centered at 425 nm, and RMMA in aniline has a shoulder at ca. 530 nm and a maximum peak at 570 nm. Using the Beer-Lambert law, the molar extinction coefficient of AMMA, NMMA, and RMMA was estimated in aniline. The molar extinction coefficient of AMMA, NMMA, and RMMA in aniline was 8845 $M^{-1}cm^{-1} \pm 6\%$ at 371 nm, 8852 $M^{-1}cm^{-1} \pm 6\%$ at 425 nm, and 80919 $M^{-1}cm^{-1} \pm 9\%$ at 570 nm, respectively.

Optical absorbance of n_1 in aniline is presented in **Figure S6d**. Using the estimated molar extinction coefficient of each emitter in aniline, the number of emitter molecules per n_1 nanoparticle could be estimated. It was estimated that one n_1 nanoparticle contained approximately 4507 molecules of AMMA, 4868 molecules of NMMA, and 1869 molecules of RMMA, corresponding to a concentration of 8.0 μM AMMA, 8.6 μM NMMA, and 3.3 μM RMMA. It should be noted that due to the very low emitter content copolymerized in the n_2 nanoparticles, no distinct peaks could be detected in the absorbance spectra of a small aliquot of n_2 nanoparticles in aniline. Larger aliquots of n_2 nanoparticles in aniline exhibited scattering such that distinct peaks were still indistinguishable.

Arrangement of emitters in the copolymerized colloidal nanoparticles

To assess the arrangement of the emitters encapsulated within the colloidal nanoparticles, a quenching study was performed using a copper(II) (Cu(II)) ion, a well known quencher for fluorescent emitters such as rhodamine B[5,6]. The PL spectra of the free RMMA emitter, an azide-modified rhodamine B derivative (azRhod) clicked to the surface of the blank polystyrene-based nanoparticles, and the n_1 nanoparticles with increasing concentrations of Cu(II) are presented in **Figure S7a-c**. The addition of Cu(II) to the free RMMA dye and azRhod surfaced-attached nanoparticles resulted in significant reductions in the PL intensity. Conversely, the addition of Cu(II) showed minimal effect on the PL intensity of the n_1 copolymerized nanoparticles. These results suggest that the copolymerized emitters are encapsulated within the nanoparticles. Additionally, these trends are consistent with a previously reported study investigating the arrangement of the NMMA dye in NMMA-copolymerized nanoparticles, where the free NMMA dye and naphthalimide surface-attached nanoparticles exhibited a decrease in PL intensity with increasing Cu(II) content while the NMMA-copolymerized nanoparticles did not[3].

Photoluminescence of the n_1, n_2, and blank polystyrene-based nanoparticles

The PL spectra of the n_1, n_2, and blank polystyrene-based nanoparticles at equivalent concentrations (ca. 1 mg/mL) is presented in **Figure S8**. While there is a very small emission detected from the blank nanoparticles centered at ca. 425 nm when excited at 370 nm, the emission of the blank nanoparticles is significantly less than that of n_1 and n_2.

Fluorescence decay measurements

A time-correlated single photon counting (TCSPC) technique was used to obtain lifetime measurements of the n_2 nanoparticles assembled in an ordered structure (OS) and corresponding disordered structure (DS). The lifetime of the nanoparticles in the OS and corresponding DS were monitored at wavelengths attributed to each emitter while the rejection wavelength (λ_{rw}) was shifted through the entire emission spectrum. It is important to note that decay profiles monitored at the λ_{rw} required significantly longer collection times than decay profiles monitored at other frequencies due to the limited spectral output at the λ_{rw}. The raw decay profiles and fits of the n_2 nanoparticles assembled in an OS and DS are shown in **Figure S9-S12**. The average measured lifetimes obtained from the decay profile fits of the n_2 nanoparticles assembled in an OS and DS are presented in **Table S2-S5**. A sample of measured lifetimes of the blank polystyrene-based nanoparticles at various wavelengths and concentrations corresponding to λ_{rw} positions in the blue, green, and red region of the visible spectrum are presented in **Table S6**.

Additional decay components of the n_2 nanoparticles in the ordered structure and disordered structure

The additional, smaller components (τ_2 and τ_3) of the double or triple exponential fits of the n_2 nanoparticles that are attributed to the polystyrene-based host material are presented in **Figure S13**.

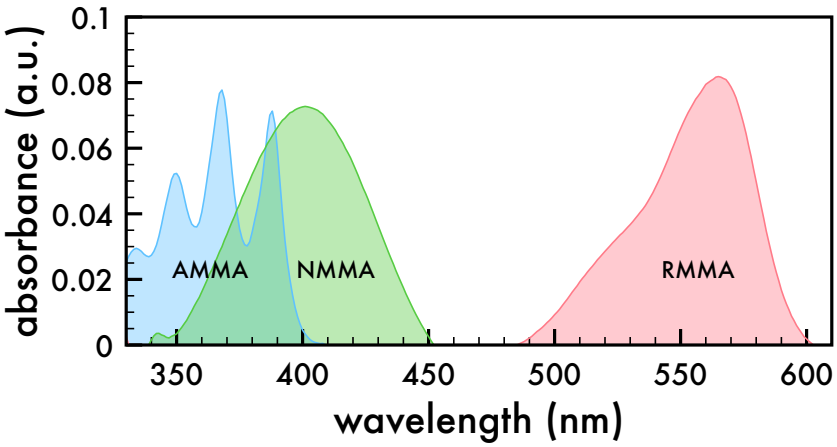

Fig. S1 Absorbance of emitters in toluene. Optical absorbance spectra of AMMA, NMMA, and RMMA in toluene at a concentration of 5 μg/mL.

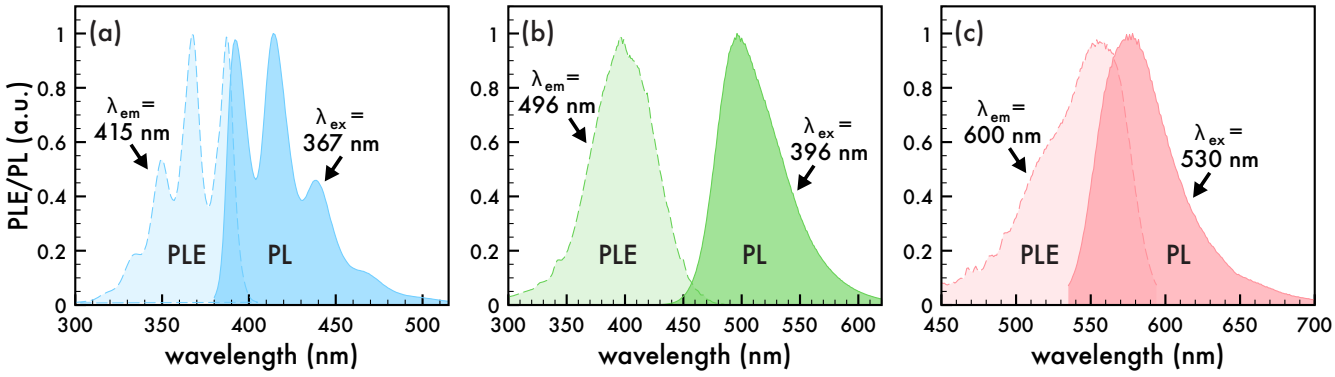

Fig. S2 Photoluminescence excitation and photoluminescence of emitters in toluene. Photoluminescence excitation (PLE) and photoluminescence (PL) spectra of (a) AMMA, (b) NMMA, and (c) RMMA at a concentration of 5 μg/mL in toluene. The emission (λ_{em}) and excitation (λ_{ex}) wavelength utilized to collect PLE and PL spectra, respectively, are indicated in (a-c).

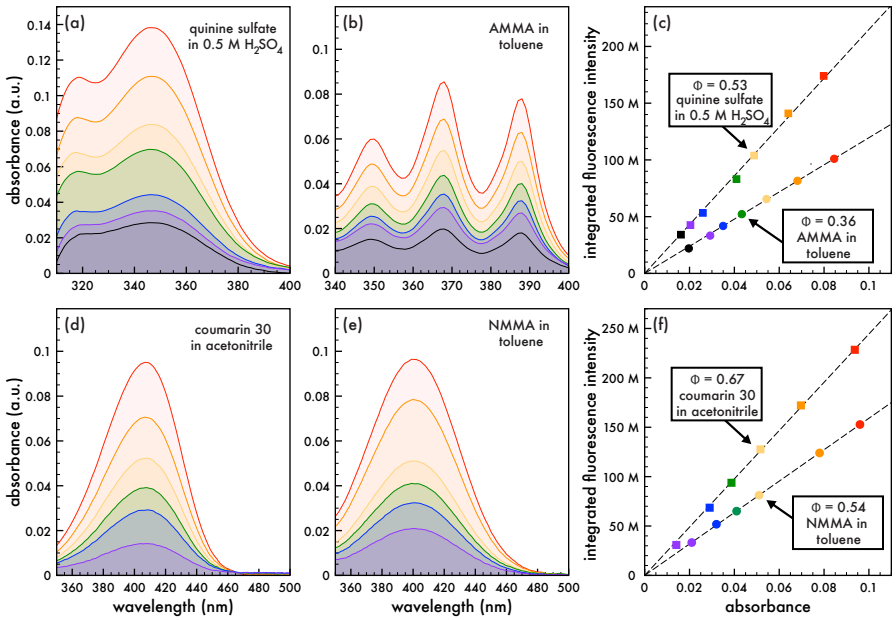

Fig. S3 Quantum yield estimations of donors. Absorbance spectra of (a) quinine sulfate in 0.5 M H_2SO_4 and (b) AMMA in toluene at decreasing concentrations (red, orange, yellow, green, blue, purple, black). (c) Integrated fluorescence intensity of quinine sulfate in 0.5 M H_2SO_4 (filled squares) and AMMA in toluene (filled circles) at decreasing concentrations (red, orange, yellow, green, blue, purple, black). The absorbance of quinine sulfate and AMMA was monitored at 367 nm and a 367 nm excitation was utilized for fluorescence measurements. A linear fit (all $R^2 = 1.00$) of the integrated fluorescence of quinine sulfate and AMMA is plotted in (e), where the gradients of each fit were utilized to estimate the quantum yield (ϕ) of AMMA in toluene. Absorbance spectra of (d) coumarin 30 in acetonitrile and (e) NMMA in toluene at decreasing concentrations (red, orange, yellow, green, blue, purple). (f) Integrated fluorescence intensity of coumarin 30 in acetonitrile (filled squares) and NMMA in toluene (filled circles) at decreasing concentrations (red, orange, yellow, green, blue, purple). The absorbance of coumarin 30 and NMMA was monitored at 403 nm and a 403 nm excitation was utilized for fluorescence measurements. A linear fit (all $R^2 = 1.00$) of the integrated fluorescence of coumarin 30 and NMMA is plotted in (e), where the gradients of each fit were utilized to estimate the ϕ of NMMA in toluene.

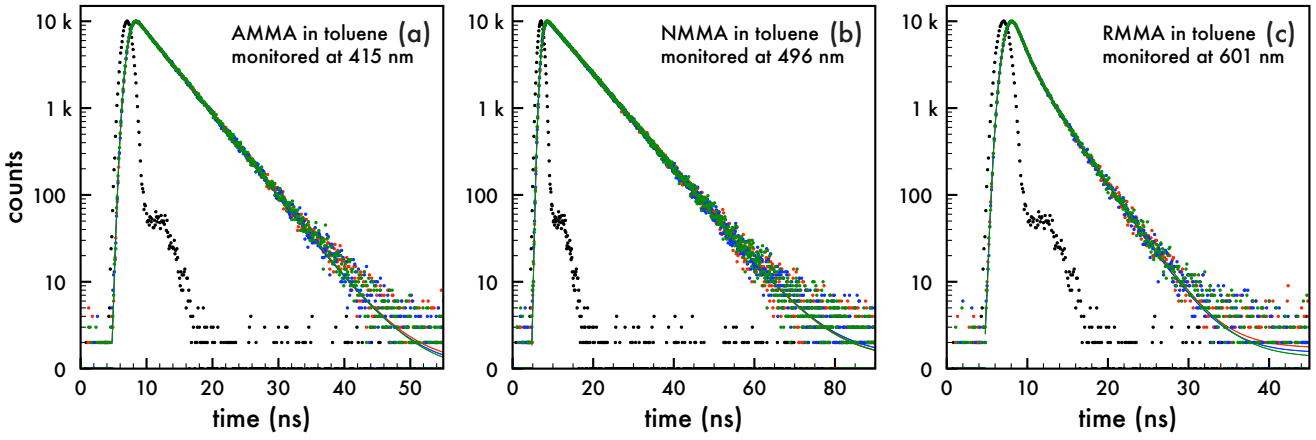

Fig. S4 Fluorescence lifetime of emitters in toluene. Decay profiles of (a) AMMA, (b) NMMA, and (c) RMMA in toluene. A 2 nm bandpass was used for all measurements and the monitored wavelength is indicated in (a-c). (a-b) were fit with a single exponential decay function and (c) was fit with a double exponential decay function.

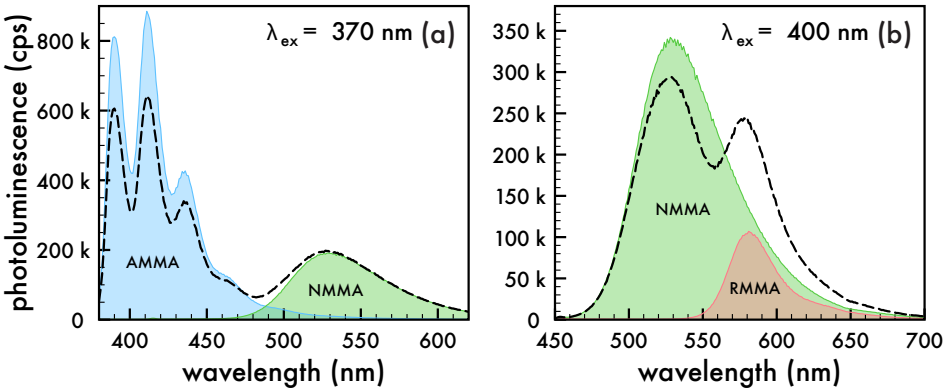

Fig. S5 Förster resonance energy transfer (FRET) between emitters. (a) Photoluminescence (PL) spectra of AMMA (blue), NMMA (green), and mixed AMMA/NMMA (black dashed line) in acetone. (b) PL spectra of NMMA (green), RMMA (red), and mixed NMMA/RMMA (black dashed line) in acetone. In all PL spectra shown in (a-b), emitters are at a concentration of 5 μg/mL.

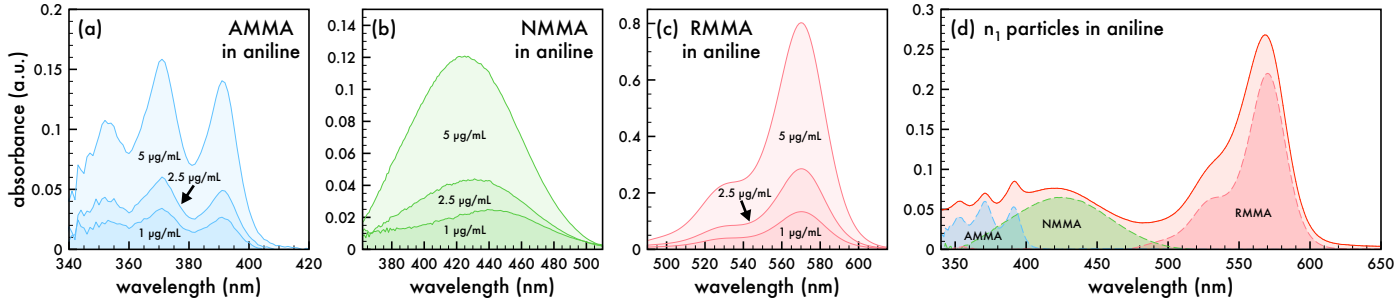

Fig. S6 Quantification of emitters in n_1 nanoparticles. Optical absorbance of (a) AMMA, (b) NMMA, and (c) RMMA in aniline at concentrations of 5 μg/mL, 2.5 μg/mL, and 1 μg/mL. (d) Optical absorbance of n_1 nanoparticles in aniline at a concentration of 1.06×10^{12} particles/mL (1.09 mg/mL). The absorbance spectra of AMMA, NMMA, and RMMA are scaled to fit under the absorbance of the nanoparticles in (d) as a visual aid.

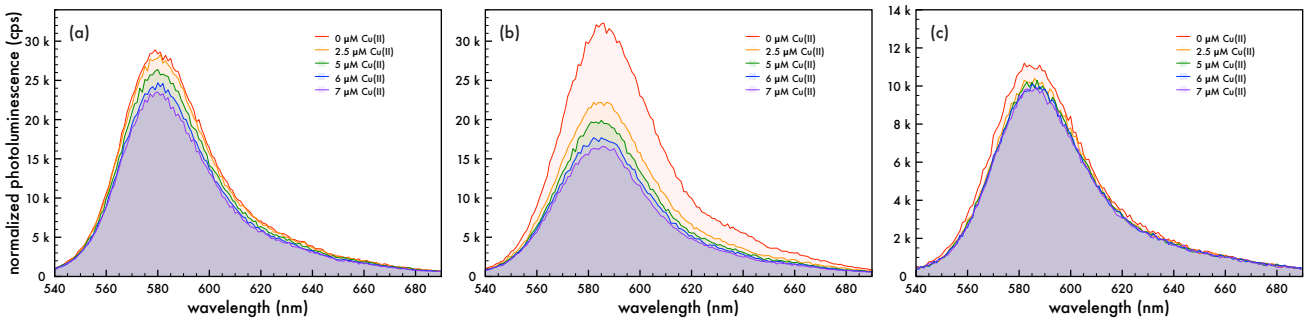

Fig. S7 Arrangement of RMMA in the n_1 nanoparticles. Photoluminescence (PL) spectra of the (a) free RMMA emitter in a 1% (v/v) solution of methanol in deionized water at a concentration of 10 μg/mL, (b) rhodamine B-clicked polystyrene-based nanoparticles in a 1% (v/v) solution of tetrahydrofuran in deionized water at a concentration of 100 μg/mL, and (c) n_1 nanoparticles in deionized water at a concentration of 10 μg/mL with increasing concentrations of Cu(II) (red, orange, green, blue, purple). A 530 nm excitation wavelength was utilized to obtain PL spectra presented in (a-c).

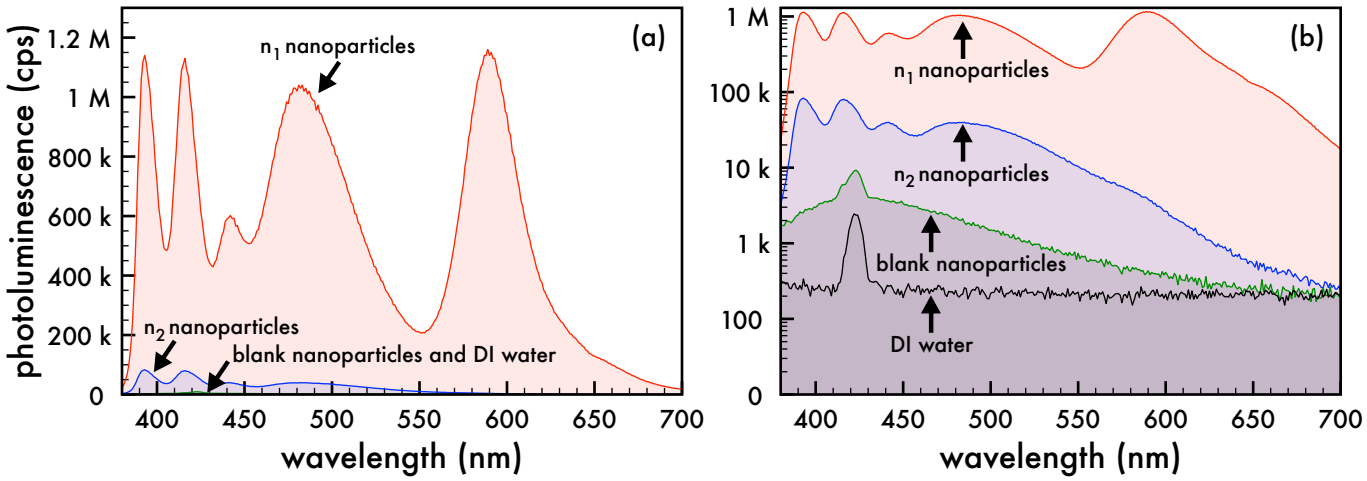

Fig. S8 Photoluminescence of n_1 n_2, and "blank" nanoparticles. (a) Photoluminescence (PL) spectra of the n_1 (red), n_2 (blue), and blank (green) polystyrene-based nanoparticles in deionized (DI) water at a concentration of 1 mg/mL. (b) PL spectra shown in (a) on a log scale for clarity. The PL spectra of DI water is also included in (a-b). A 370 nm excitation wavelength was utilized to obtain PL spectra presented in (a-b).

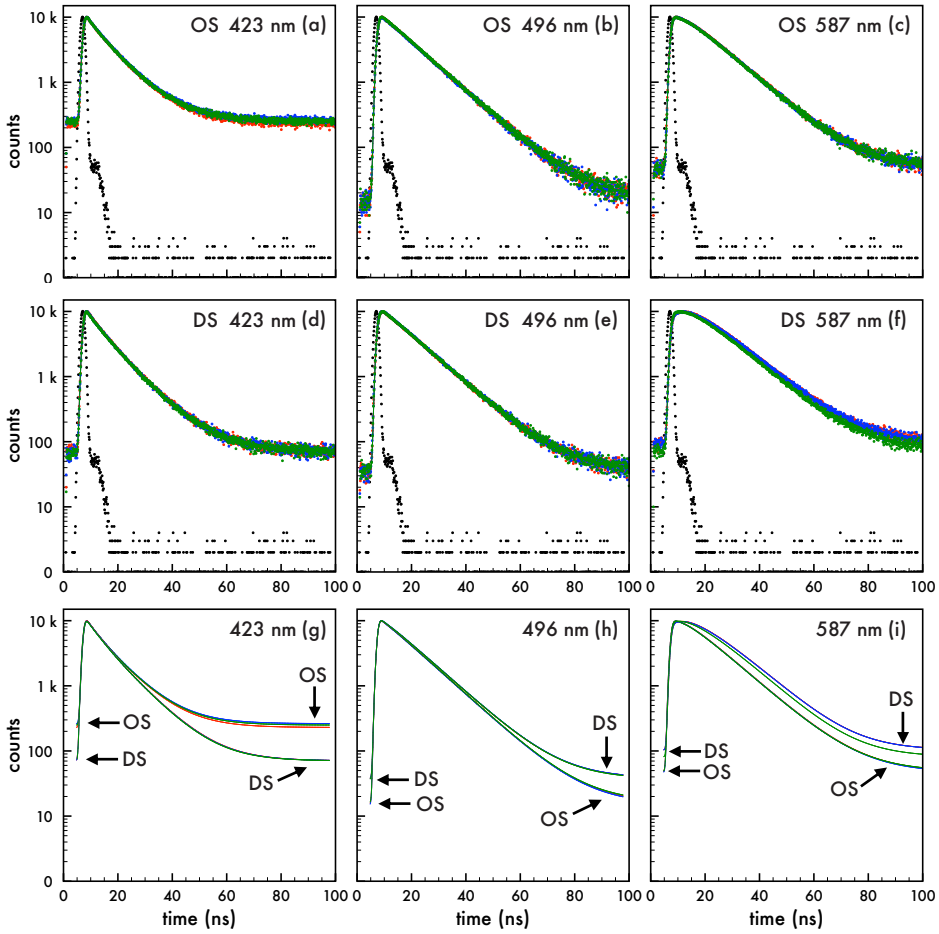

Fig. S9 Decay profiles of n_2 nanoparticles when the λ_{rw} was overlapping AMMA. Decay profiles collected to a decay profile peak maximum of 10000 counts (P_{10K}) of n_2 nanoparticles assembled in (a-c) an ordered structure (OS) and (d-f) a disordered "reference" structure (DS) when the rejection wavelength (λ_{rw}) was at 423 nm. Decay profiles were monitored at (a,d) 423 nm, (b,e) 496 nm, and (c,f) 587 nm. The instrument response using Ludox (black dots) and monitored at 370 nm is included in (a-f). Exponential fits for OS and DS when the λ_{rw} was at 423 nm and monitored at (g) 423 nm, (h) 496 nm, and (i) 587 nm. A 2 nm bandpass was used for all measurements and all fits are double exponential decay functions.

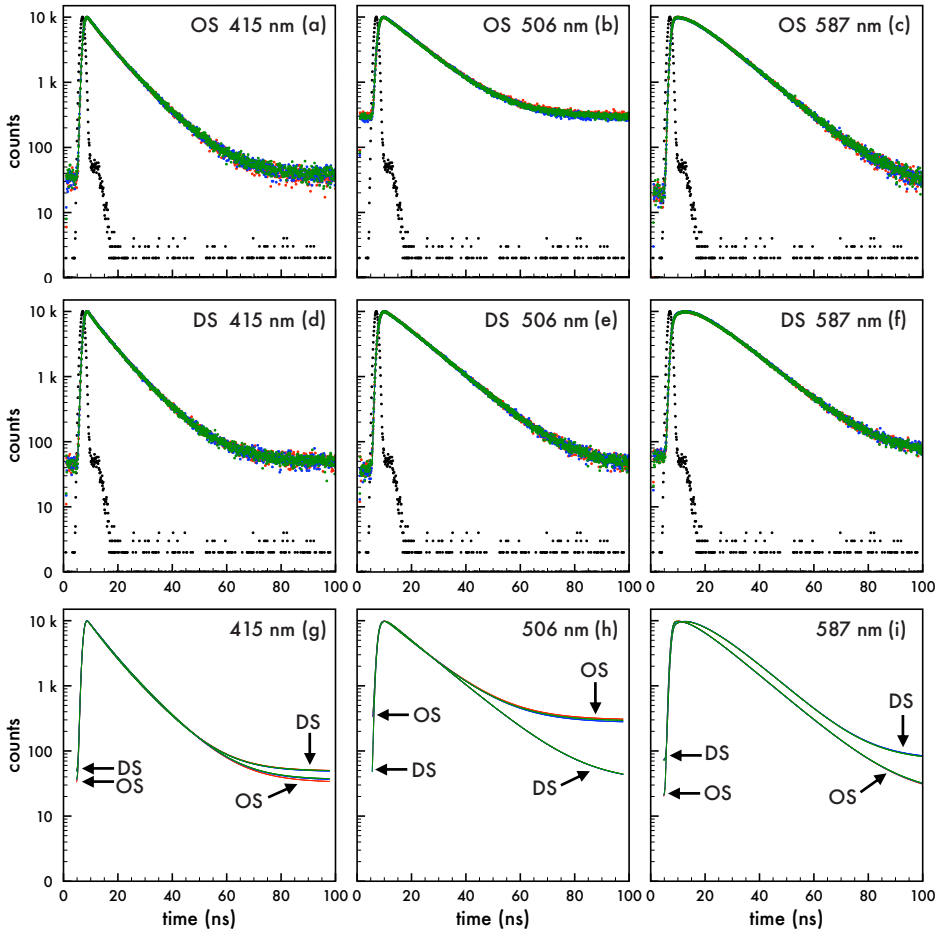

Fig. S10 Decay profiles of n_2 nanoparticles when the λ_{rw} was overlapping NMMA. Decay profiles collected to a decay profile peak maximum of 10000 counts (P_{10K}) of n_2 nanoparticles assembled in (a-c) an ordered structure (OS) and (d-f) a disordered "reference" structure (DS) when the rejection wavelength (λ_{rw}) was at 506 nm. Decay profiles were monitored at (a,d) 415 nm, (b,e) 506 nm, and (c,f) 587 nm. The instrument response using Ludox (black dots) and monitored at 370 nm is included in (a-f). Exponential fits for OS and DS when the λ_{rw} was at 506 nm and monitored at (g) 415 nm, (h) 506 nm, and (i) 587 nm. A 2 nm bandpass was used for all measurements and all fits are double exponential decay functions.

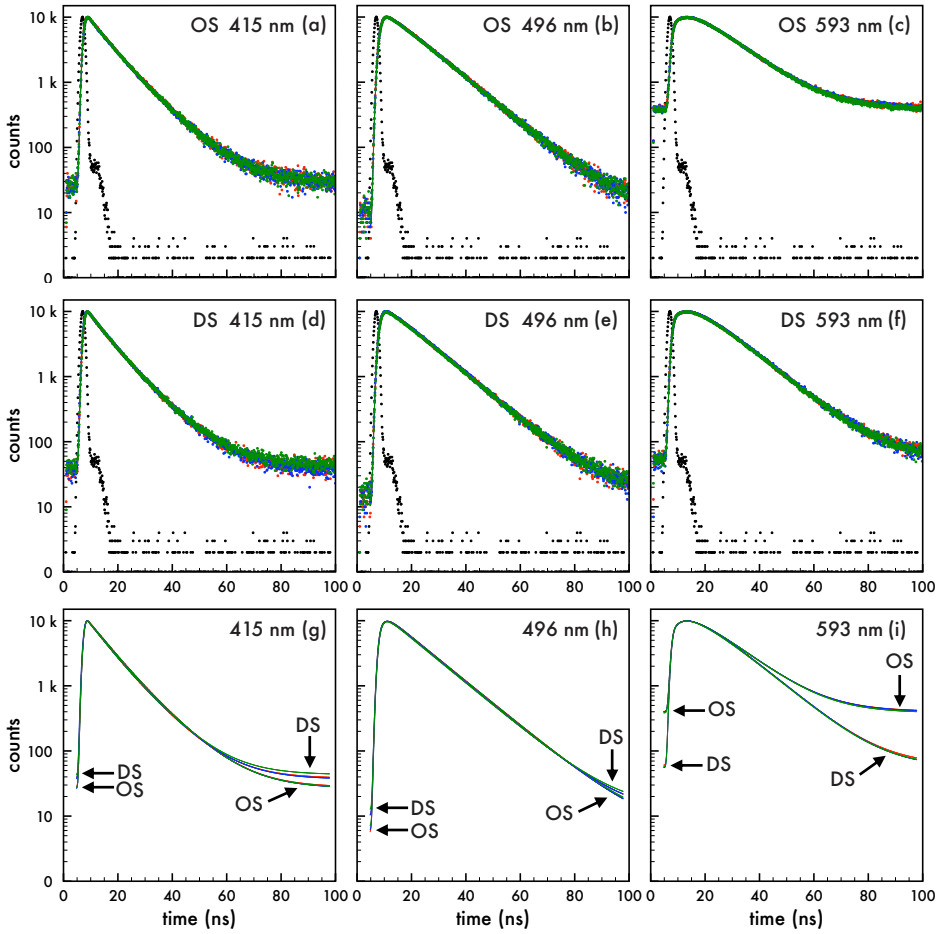

Fig. S11 Decay profiles of n_2 nanoparticles when the λ_{rw} was overlapping RMMA. Decay profiles collected to a decay profile peak maximum of 10000 counts (P_{10K}) of n_2 nanoparticles assembled in (a-c) an ordered structure (OS) and (d-f) a disordered "reference" structure (DS) when the rejection wavelength (λ_{rw}) was at 593 nm. Decay profiles were monitored at (a,d) 415 nm, (b,e) 496 nm, and (c,f) 593 nm. The instrument response using Ludox (black dots) and monitored at 370 nm is included in (a-f). Exponential fits for OS and DS when the λ_{rw} was at 593 nm and monitored at (g) 415 nm, (h) 496 nm, and (i) 593 nm. A 2 nm bandpass was used for all measurements. (g,h) are double exponential decay functions and (i) is a triple exponential decay function.

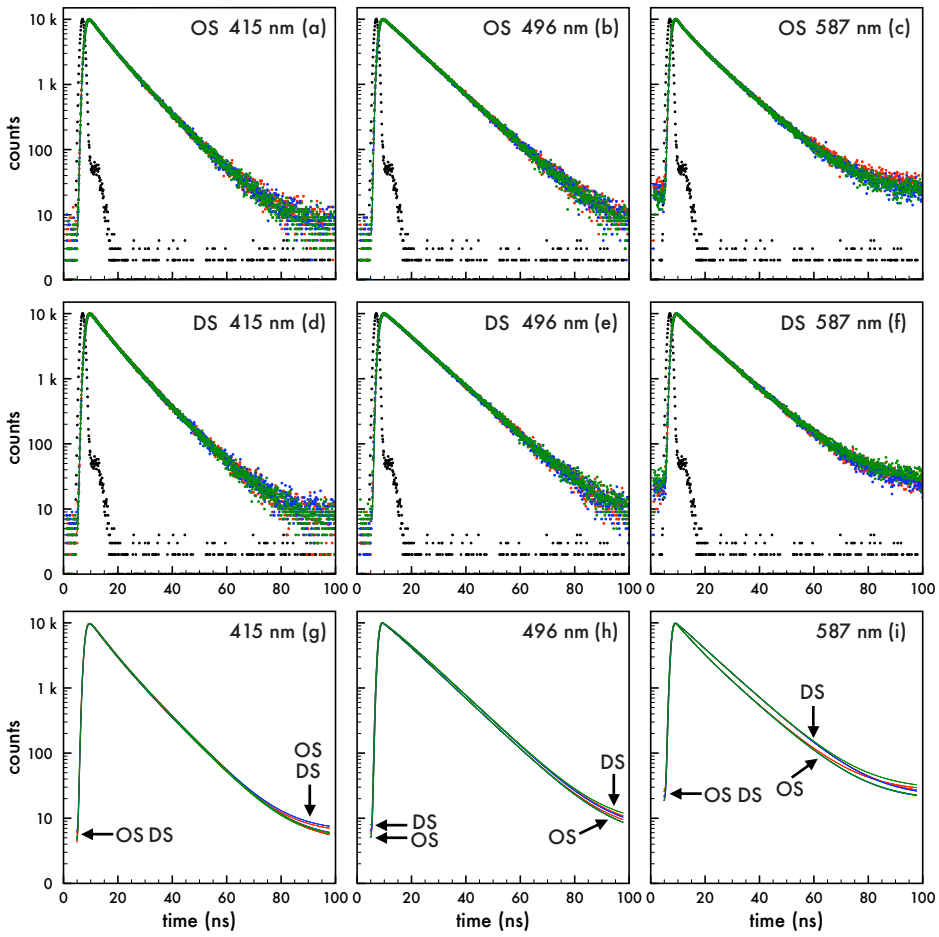

Fig. S12 Decay profiles of n_2 nanoparticles when the λ_{rw} was not overlapping the emission. Decay profiles collected to a decay profile peak maximum of 10000 counts (P_{10K}) of n_2 nanoparticles assembled in (a-c) an ordered structure (OS) and (d-f) a disordered "reference" structure (DS) when the rejection wavelength (λ_{rw}) was at 823 nm. Decay profiles were monitored at (a,d) 415 nm, (b,e) 496 nm, and (c,f) 587 nm. The instrument response using Ludox (black dots) and monitored at 370 nm is included in (a-f). Exponential fits for OS and DS when the λ_{rw} was at 823 nm and monitored at (g) 415 nm, (h) 496 nm, and (i) 587 nm. A 2 nm bandpass was used for all measurements. (g) is a triple exponential decay function and (h,i) are double exponential decay function.

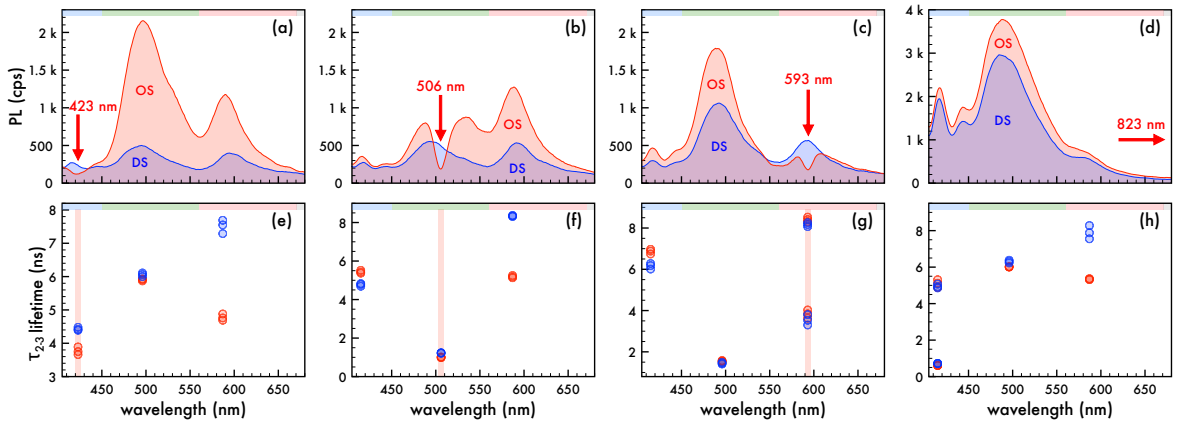

Fig. S13 Smaller decay components (τ_{2-3}) of the n_2 nanoparticles. Photoluminescence (PL) of n_2 assembled in an ordered structure (OS, red) as the rejection wavelength (λ_{rw}) was shifted to (a) 423 nm, (b) 506 nm, (c) 593 nm, and (d) 823 nm compared to the corresponding disordered structure (DS, blue). A 370 nm excitation wavelength was utilized to obtain PL spectra presented in (a-d). Average ($n = 3$) measured lifetime (τ_{2-3}) of spectral regions attributed to each emitter in the OS (red circles) as the λ_{rw} was shifted to (e) 423 nm, (f) 506 nm, (g) 593 nm, and (h) 823 nm compared to the corresponding DS (blue circles). The spectral regions attributed to AMMA (blue), NMMA (green), RMMA (red) emission are lightly shaded at the top of (a-h) as a visual aid.

emitter - λ (nm)	α (%)	χ^2	RA (%)	τ_1 (ns)	$\pm$ (ns)	RA (%)	τ_2 (ns)	$\pm$ (ns)
AMMA - 415	1.30	1.14	100.0	4.56	0.03	-	-	-
NMMA - 496	1.50	1.04	100.0	7.88	0.01	-	-	-
RMMA - 601	0.57	1.09	49.0	1.21	0.04	51.0	3.28	0.06

Table S1 Fluorescence lifetime of emitters in toluene. Average (at least $n = 3$) measured lifetimes ($\tau_{1-2} \pm$ stdev) of AMMA, NMMA, and RMMA in toluene at 415 nm, 496 nm, and 601 nm, respectively. The average relative amplitude (RA) of each lifetime in the decay function is indicated prior to each measured lifetime value. All decay profiles were collected to P_{10k} and fit (χ^2) to a single or double exponential decay function. The average α of each data set indicated.

λ (nm)	α (%)	χ^2	RA (%)	τ_1 (ns)	$\pm$ (ns)	RA (%)	τ_2 (ns)	$\pm$ (ns)
423_O	0.01	1.01	85.1	9.83	0.05	14.9	3.75	0.13
423_D	0.03	1.04	79.6	10.15	0.08	20.4	4.42	0.05
496_O	0.20	1.18	105.5	11.37	0.02	-5.5	5.91	0.03
496_D	0.08	1.65	111.0	11.30	0.02	-11.0	6.06	0.06
587_O	0.09	0.99	120.8	11.74	0.04	-20.8	4.76	0.10
587_D	0.05	1.37	225.3	10.87	0.01	-125.3	7.55	0.22

Table S2 Fluorescence lifetime of n_2 nanoparticles when the λ_{rw} was overlapping AMMA. Average (at least $n = 3$) measured lifetimes ($\tau_{1-2} \pm$ stdev) of the n_2 nanoparticles assembled in an ordered structure (OS, λ_O) and disordered structure (DS, λ_D) when the λ_{rw} was at 423 nm (gray). The average relative amplitude (RA) of each lifetime in the decay function is indicated prior to each measured lifetime value. All decay profiles were collected to P_{10k} and fit (χ^2) to a double exponential decay function. The average α of each data set indicated.

λ (nm)	α (%)	χ^2	RA (%)	τ_1 (ns)	$\pm$ (ns)	RA (%)	τ_2 (ns)	$\pm$ (ns)
415_O	0.06	1.02	73.5	10.36	0.03	27.2	5.43	0.08
415_D	0.05	1.04	76.6	9.99	0.05	23.4	4.78	0.08
506_O	0.01	1.17	108.7	12.34	0.03	-8.7	1.00	0.02
506_D	0.08	1.36	108.4	12.57	0.02	-8.4	1.23	0.02
587_O	0.23	1.07	130.5	12.23	0.02	-30.5	5.18	0.06
587_D	0.09	1.87	350.0	10.45	0.01	-250.0	8.34	0.03

Table S3 Fluorescence lifetime of n_2 nanoparticles when the λ_{rw} was overlapping NMMA. Average (at least $n = 3$) measured lifetimes ($\tau_{1-2} \pm$ stdev) of the n_2 nanoparticles assembled in an ordered structure (OS, λ_O) and disordered structure (DS, λ_D) when the λ_{rw} was at 506 nm (gray). The average relative amplitude (RA) of each lifetime in the decay function is indicated prior to each measured lifetime value. All decay profiles were collected to P_{10k} and fit (χ^2) to a double exponential decay function. The average α of each data set indicated.

λ (nm)	α (%)	χ^2	RA (%)	τ_1 (ns)	$\pm$ (ns)	RA (%)	τ_2 (ns)	$\pm$ (ns)	RA (%)	τ_3 (ns)	$\pm$ (ns)
415_O	0.08	1.28	52.1	11.37	0.18	47.9	6.88	0.12	-	-	-
415_D	0.05	1.07	60.2	10.84	0.13	39.8	6.18	0.15	-	-	-
496_O	0.33	1.57	114.2	12.73	0.03	-15.9	1.55	0.03	-	-	-
496_D	0.18	1.40	112.2	12.60	0.01	-12.2	1.45	0.04	-	-	-
593_O	0.01	1.03	241.9	11.40	0.15	-129.4	8.41	0.38	-12.5	3.84	0.14
593_D	0.09	1.21	216.6	11.60	0.03	-105.1	8.17	0.16	-11.5	3.53	0.13

Table S4 Fluorescence lifetime of n_2 nanoparticles when the λ_{rw} was overlapping RMMA. Average (at least $n = 3$) measured lifetimes ($\tau_{1-3} \pm$ stdev) of the n_2 nanoparticles assembled in an ordered structure (OS, λ_O) and disordered structure (DS, λ_D) when the λ_{rw} was at 593 nm (gray). The average relative amplitude (RA) of each lifetime in the decay function is indicated prior to each measured lifetime value. All decay profiles were collected to P_{10k} and fit (χ^2) to a double or triple exponential decay function. The average α of each data set indicated.

λ (nm)	α (%)	χ^2	RA (%)	τ_1 (ns)	$\pm$ (ns)	RA (%)	τ_2 (ns)	$\pm$ (ns)	RA (%)	τ_3 (ns)	$\pm$ (ns)
415_O	0.43	1.05	78.9	10.17	0.08	30.0	5.12	0.22	-8.9	0.61	0.01
415_D	0.35	1.23	82.3	10.16	0.11	28.4	4.93	0.12	-10.7	0.72	0.01
496_O	0.61	1.98	106.6	10.96	0.02	-6.6	6.01	0.02	-	-	-
496_D	0.56	3.11	113.9	10.95	0.00	-13.9	6.31	0.08	-	-	-
587_O	0.11	1.44	80.8	11.75	0.03	19.2	5.34	0.03	-	-	-
587_D	0.10	1.69	92.4	11.75	0.06	7.4	7.88	0.37	-	-	-

Table S5 Fluorescence lifetime of n_2 nanoparticles when the λ_{rw} was not overlapping the emission. Average (at least $n = 3$) measured lifetimes (τ_{1-3} $\pm$ stdev) of the n_2 nanoparticles assembled in an ordered structure (OS, λ_O) and disordered structure (DS, λ_D) when the λ_{rw} was at 823 nm (gray). The average relative amplitude (RA) of each lifetime in the decay function is indicated prior to each measured lifetime value. All decay profiles were collected to P_{10k} and fit (χ^2) to a double or triple exponential decay function. It should be noted that 496_D did not fit well to a triple exponential decay function, which is why a double exponential decay function was used. The average α of each data set indicated.

λ_{rw} position (nm)	λ (nm)	α (%)	χ^2	RA (%)	τ_1 (ns)	$\pm$ (ns)	RA (%)	τ_2 (ns)	$\pm$ (ns)	RA (%)	τ_3 (ns)	$\pm$ (ns)
486	475	0.01	1.30	67.3	8.29	0.1	4488.7	2.02	0.2	-4456.0	2.00	0.02
486	486	0.01	1.41	75.1	8.44	0.09	1285.2	1.91	0.19	-1260.3	1.85	0.02
486	520	0.01	1.26	82.8	8.50	0.05	63.4	2.16	0.16	-46.3	1.17	0.02
536	520	0.01	1.24	78.1	8.84	0.06	52.2	2.54	0.13	-30.3	0.98	0.02
536	536	0.01	1.28	82.7	8.32	0.05	46.7	2.18	0.14	-29.4	0.92	0.02
536	560	0.01	1.16	77.6	8.78	0.06	36.3	2.60	0.12	-13.9	0.57	0.02
585	530	0.01	1.09	79.1	8.56	0.05	45.7	2.39	0.11	-24.8	0.85	0.02
585	585	0.01	0.95	72.5	8.74	0.09	40.2	2.71	0.12	-12.8	0.51	0.02
642	550	0.01	1.09	75.8	8.83	0.06	41.8	2.61	0.11	-17.7	0.66	0.02

Table S6 Sample of fluorescence lifetimes of "blank" nanoparticles at various nanoparticle concentrations corresponding to λ_{rw} positions in the visible spectrum. Measured lifetimes (τ_{1-3} $\pm$ stdev) of a sample of blank polystyrene-based nanoparticles at various concentrations corresponding to the indicated λ_{rw} positions. All decay profiles were collected to P_{10k} and fit (χ^2) to a triple exponential decay function. The average relative amplitude (RA) of each lifetime in the decay function is indicated prior to each measured lifetime value and the average α of each data set indicated.

References

1 A. Williams, S. Winfield and J. Miller, *Analyst*, 1983, **108**, 1067–1071.

2 M. J. Adams, J. G. Highfield and G. F. Kirkbright, *Analytical Chemistry*, 1977, **49**, 1850–1852.

3 H. W. Jones, Y. Bandera and S. H. Foulger, *ACS Omega*, 2024, **accepted**, https://doi.org/10.1021/acsomega.4c07335.

4 G. Jones, W. Jackson and C. Choi, *J Phys Chem*, 1985, **89**, 294–300.

5 J. Ding, L. Yuan, L. Gao and J. Chen, *Journal of Luminescence*, 2012, **132**, 1987–1993.

6 N. Doumani, E. Bou-Maroun, J. Maalouly, M. Tueni, A. Dubois, C. Bernhard, F. Denat, P. Cayot and N. Sok, *Sensors*, 2019, **19**, 4514.